Impurity Ion Complexation Enhances Carbon Dioxide Reduction Catalysis

Citation: Wuttig, Anna, and Yogesh Surendranath. "Impurity Ion Complexation Enhances Carbon Dioxide Reduction Catalysis." ACS Catalysis 5, no. 7 (July 2, 2015): 4479-4484.

As Published: http://dx.doi.org/10.1021/acscatal.5b00808

Publisher: American Chemical Society (ACS)

Persistent URL: http://hdl.handle.net/1721.1/103935

Version: Author's final manuscript: final author's manuscript post peer review, without publisher's formatting or copy editing

Impurity Ion Complexation Enhances Carbon Dioxide Reduction Catalysis

Anna Wuttig and Yogesh Surendranath*

Department of Chemistry, Massachusetts Institute of Technology, Cambridge, Massachusetts 02139

ABSTRACT: Herein, we show that group 11 CO_2 reduction catalysts are rapidly poisoned by progressive deposition of trace metal ion impurities existent in high purity electrolytes. Metal impurity deposition was characterized by XPS and in situ stripping voltammetry and is coincident with loss of catalytic activity and selectivity for CO_2 reduction, favoring hydrogen evolution on poisoned surfaces. Metal deposition can be suppressed by complexing trace metal-ion impurities with ethylenediaminetetraacetic acid or solid supported iminodiacetate resins. Metal ion complexation allows for reproducible, sustained catalytic activity and selectivity for CO_2 reduction on Au, Ag, and Cu electrodes. Together, this study establishes the principle mode by which group 11 CO_2 reduction catalysts are poisoned and lays out a general approach for extending the lifetime of electrocatalysts subject to impurity metal deposition.

1. INTRODUCTION

Catalytic reactions are highly sensitive to the presence of impurities. Trace constituents in the reaction medium can have an outsized effect on reaction efficiency and selectivity by interfering with the active species or mediating turnover by themselves. For example, metal and halide contaminants promote and poison product activity and selectivity in a myriad array of heterogeneous reactions[1–4], have led to serendipitous catalyst discovery in organic synthesis[5,6], and can dramatically alter enzymatic activity[7–9].

Trace impurities also play a dominant role in electrochemical energy catalysis. For example, trace Co^{2+} impurities have lead to false-positives in the development of molecular oxygen evolution reaction (OER) catalysts[10] and trace iron[11,12] and platinum[13] impurities have been shown to enhance the OER on heterogeneous catalysts. Likewise, Pt surfaces are readily poisoned for the oxygen reduction reaction (ORR) by various impurities[14] whereas "metal-free" ORR activity has been ascribed to trace metal impurities.[15] Trace metal impurities have also been shown to convolute the facet-dependence of hydrogen evolution reaction (HER) activity on Au surfaces.[16]

The electrochemical reduction of CO_2 to fuels is of growing interest because it provides an attractive platform for the storage of intermittent renewable energy in energy dense chemical bonds.[17–19] Relative to other energy conversion reactions such as ORR, OER, and HER, CO_2 reduction (CDR) is particularly sensitive to surface structure and composition because of the myriad array of CDR products thermodynamically accessible over a narrow potential range.[20–22] The development of practical CDR catalysts requires unparalleled control over product selectivity, which can be easily compromised by impurities that interact with or irreversibly alter the surface.

Group 11 metal surfaces are regarded as the most promising heterogeneous catalysts for this reaction because they display low to moderate overpotentials for CO production, and, in the case of copper, generate higher order products including methane and ethylene.[23–31] However, planar group 11 metal surfaces are known to lose their catalytic activity and selectivity for CO_2 reduction over the time scale of minutes to hours under steady state electrolysis.[22,32–37] For example, copper surfaces lose one-half of their catalytic activity for methane production within 20 min of polarization,[33,35] and CO production selectivity on Au[32] and Ag[34] decreases within minutes of electrolysis. Despite posing a clear obstacle to practical implementation of CO_2 reduction technologies, the mechanistic basis for this activity loss remains poorly understand.

Researchers have posited that the deactivation is due the deposition of trace metal ion[22,35] or organic impurities[35] in the electrolyte, and others have suggested that this is activity loss is unavoidably, resulting from the accumulation of catalytic intermediates that poison the surface over time[22,33,38–41]. Based on these hypotheses, contemporary strategies to prolonging catalyst lifetimes include periodic oxidative pulsing of the electrode to remove adsorbed organics[32–34] and long-term (>9 hrs) pre-electrolysis using a sacrificial electrode to scavenge trace metal ion impurities in the electrolyte.[35] The former is impractical because it progressively alters the catalyst surface structure[42], and pre-electrolysis has been shown, in many cases, to be ineffective[43,44] and irreproducible,[33,34] and is both energy and time intensive. We note that high surface electrodes[37,38,44,45] should exhibit reduced sensitivity to trace impurities, but these systems are difficult to probe mechanistically, due to their complex morphology and structure. Thus, the systematic development of new CDR catalysts would benefit from a clear understanding of the principle CDR deactivation mechanism on these surfaces and the development of simple strategies for sustaining catalyst activity and selectivity over time.

Herein, we demonstrate, unambiguously, that metal ion deposition is the principle mode of catalyst deactivation for Cu, Ag, and Au metal surfaces and show, for the first time, that catalyst deactivation can be entirely eliminated by irre-

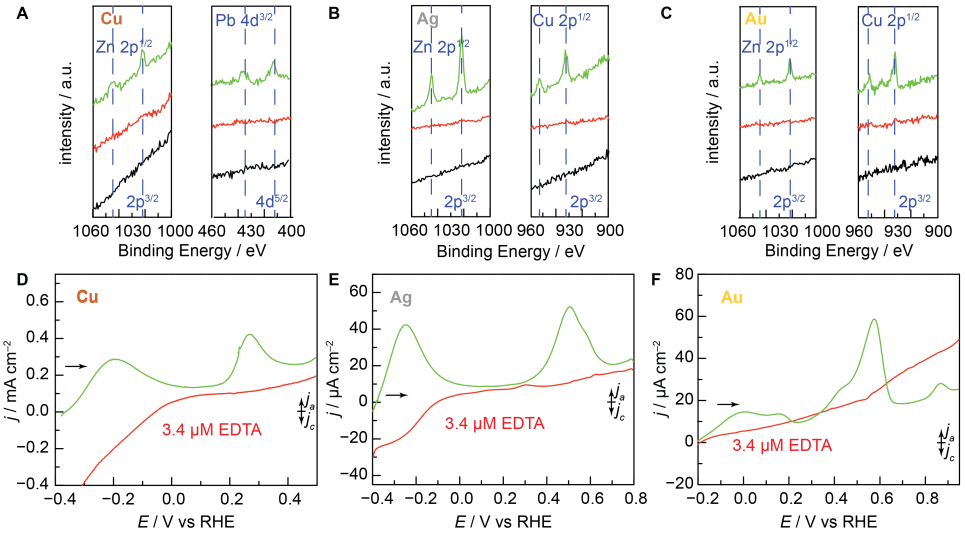

Figure 1. Surface chemistry following CDR catalysis on group 11 metal surfaces. Narrow scan X-ray photoelectron spectra of Cu (**A**), Ag (**B**), and Au (**C**) rotating electrodes before (**black**) catalysis and after 45 min of CDR catalysis in native C_i electrolyte (**green**) and EDTA-containing electrolyte (**red**). Cyclic voltammetry traces of rotating electrodes at 2500 RPM in native C_i electrolyte (**green**) or EDTA-containing C_i electrolyte (**red**) after (**D**) 120 min of CDR catalysis at −1.00 V on Cu; (**E**) 45 min of CDR catalysis at −0.90 V on Ag; and (**F**) 45 min of CDR catalysis at −0.70 V on Au. In all cases, CV scans were recorded at 50 mV s^{-1} scan rate with a positive direction of scan.

versibly coordinating trace metal ions *in situ* with ethylenediaminetetraacetic acid (EDTA) or *ex situ* with a solid-supported iminodiacetate resin. The high binding affinity[46] and rapid complexation kinetics ($k_1 \approx 10^{10}$ $M^{-1}s^{-1}$)[47–50] of EDTA and solid phase analogues make this a general strategy for maintaining high CDR activity over time, regardless of structure of the catalyst.

2. RESULTS AND DISCUSSION

Group 11 Surfaces Accumulate Impurity Metal Poisons During CO_2 Reduction Catalysis. To characterize the purity of group 11 surfaces following CDR catalysis, we analysed electrodes by X-ray photoelectron spectroscopy (XPS) following electrolysis in unpurified CO_2-saturated 0.1 M $NaHCO_3$ (C_i) electrolyte (full experimental details, including solution, electrode and electrochemical cell preparation, are available in the SI). Despite using 18 MΩ cm water and electrolyte salts of the highest purity (99.9999%, Aldrich TraceSELECT) available commercially, XPS of copper rotating disk electrodes following 45 min of electrolysis at potentials typical for selective CO_2 reduction, (−1.0 V, all potentials are quoted versus the reversible hydrogen electrode, RHE), reveals the build-up of zinc and lead impurities (Figures 1A and S1). Similarly, prolonged electrolyses of silver (−0.9 V) and gold (−0.7 V) rotating cone electrodes reveal the accumulation of zinc and copper impurities, (Figures 1B, C and S1). Previous studies conducted at similar electrolysis potentials were unable to detect trace metal impurity signals via XPS.[25] Our use of a rotating electrode serves to accelerate the rate of diffusion-limited metal deposition, increasing the surface impurity population (see SI calculation). These XPS results indicate that all group 11 metal surfaces are subject to contamination via impurity deposition even in cases where high purity electrolytes are employed. These results are in line with the relatively high thermodynamic $M^{2+/0}$ redox potentials for Cu^{2+}(0.75 V) and Pb^{2+}(0.28 V) and Zn^{2+} (−0.35 V)[51] under CDR conditions and the detection of μM concentrations of Zn^{2+} by Inductively Coupled Plasma Mass Spectrometry. Given that the thermodynamic potentials for metal deposition are close to or positive of the thermodynamic potentials for CDR catalysis, we expect that impurity deposition will also occur on high surface area group 11 catalysts that operate at lower CDR overpotentials, albeit at slower rates.

To gain further insight into changes in surface composition during CDR catalysis, we characterized electrodes via cyclic voltammetry (CV) immediately following (~1 s time delay) reductive polarization. The first CV sweeps recorded after short (15 min) and prolonged (>45 min) CDR catalysis in native C_i electrolyte reveal a progressive rise, Figure S2A, in broad oxidative features at −0.22 V and 0.26 V for Cu, Figures 1D (green). Likewise, for Ag electrodes, we observe a continuous rise, Figure S2B, in broad oxidative features at −0.25 V and 0.50 V, Figures 1E (green). A similar experiment on Au reveals a rise, Figure S2C, of features at 0.11 V, 0.50 V, and 0.85 V with the appearance of distinct shoulders upon longer electrolysis, Figure 1F (green). These features are not observed prior to CDR catalysis (Figure S2A-C, black) or upon subsequent cycling of the electrode after CDR catalysis. Together, the observations suggest that these waves originate from irreversible oxidative stripping ($M^0 \rightarrow M^{n+} + ne^-$) of impurity metals electrodeposited on Cu, Ag, and Au surfaces during CDR catalysis.

To assign these stripping waves to metal ion impurities, we collected CV traces following CDR in C_i electrolyte, containing 50μM of various M^{2+} salts of metals detected via XPS. This intentional introduction of an impurity metal ion allows us to probe the stripping behaviour of a single M^{2+} candidate under experimental conditions relevant to CDR catalysis. For Cu electrodes polarized at CDR potentials in Zn^{2+} containing electrolytes, the first CV scan following CDR catalysis reveals a broad Zn stripping feature at −0.30 V, Figure S3A (red), in line with one oxidative wave, at −0.22 V, Figure 1D (green),

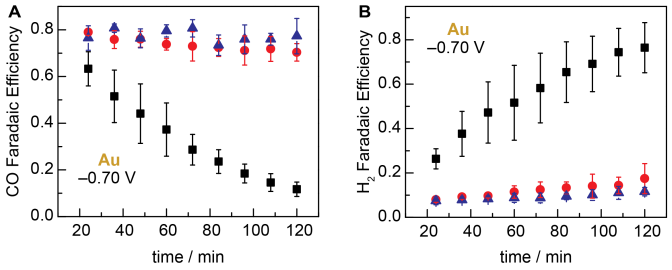

Figure 2. Faradaic efficiencies for CDR and HER product formation on gold foil in electrolytes of varying purity. Activity of Au for CO (**A**) and H_2 (**B**) formation at −0.70 V in native C_i electrolyte (**black squares**), C_i electrolyte containing 3.4 μM EDTA (**red circles**), and Chelex-treated C_i electrolyte (**blue triangles**).

observed for CDR performed in native C_i electrolyte. An analogous experiment performed with Pb^{2+} containing electrolyte reveals oxidative features at 0.15 V and 0.26 V (Figure S3A, blue), attributed to stripping of bulk and underpotential deposited (UPD) lead on Cu, as previously characterized in acidic electrolytes.[52] Consistent with the low concentrations of Pb in native C_i electrolyte (Table S1), the stripping feature observed in Figures 1D (green) matches the UPD stripping potential of 0.26 V in Figure S3A (blue). Together these results indicate that Cu is susceptible to progressive fouling by Zn and Pb deposition during CDR catalysis.

Similar experiments conducted with Ag and Au working electrodes in Zn^{2+} containing electrolytes reveal Zn stripping features at −0.35 V and −0.23 V for Ag (Figure S3B, red), and at −0.10 V and 0.12 V for Au (Figure S3C, red). In both cases, the more positive peak is attributed to Zn UPD stripping features,[53–55] which match the stripping waves at −0.25 V on Ag (Figure 1E, green) and 0.11 V on Au (Figure 1F, green) observed following CDR in native C_i electrolyte. Analogous experiments performed with Ag and Au electrodes in Cu^{2+} containing electrolytes reveal broad stripping features at 0.50 V and 0.60 V for Ag (Figure S3B, green), and 0.65 V and 0.85V for Au (Figure S3C, green). These features are close to the stripping waves observed at 0.50 V on Ag (Figure 1E, green), and 0.56 V and 0.85 V on Au (Figure 1F, green) following CDR in native C_i electrolyte. Slight differences in potentials may be due to alloying of co-deposited Cu and Zn from native C_i electrolytes,[56] as opposed to the deposition of Cu alone from Cu^{2+} enriched electrolytes. Stripping features for other common first row transition metals, such as Fe and Ni, would be expected to occur at values less positive than that of Cu,[51,57]leading us to assign the aforementioned peaks to Cu stripping. Together with XPS data, analysis of stripping voltammograms demonstrates that group 11 electrodes are susceptible to fouling by Pb, Zn, and Cu deposition during CDR catalysis.

Chelation Inhibits Impurity Deposition and Enables Sustained CO_2 Reduction Catalysis. Impurity metal deposition leads to dramatic changes in CDR selectivity on group 11 catalysts. At −0.70 V, CO production on polycrystalline Au foil electrodes operated in native C_i electrolytes commences with ~60% Faradaic efficiency but declines to ~10% over the course of 2 hours (Figure 2A, black squares, error bars shown in Figures 2-4 are the standard deviation of three independent measurements) consistent with literature reports.[32,34] The large error bars observed for electrolyses performed in native C_i electrolyte reveal a high degree of run-to-run variability, consistent with trace metal impurities strongly influencing catalytic efficiency. Catalyst deactivation for CO production is accompanied by a rise, from ~23% to ~77%, in Faradaic efficiency for the hydrogen evolution reaction (HER). The observed CO and H_2 account for ~90% of the steady state current, and no other gas phase products (see SI for experimental details) were detected, suggesting that solution phase products, such as formate,[23] may account for the balance. Notwithstanding, CDR selectivity is progressively eroded over time for electrolysis performed from native C_i electrolyte. In order to supress the observed deactivation, we employed established preelectrolysis methods[35] to clean the electrolyte. In our hands, this method proved ineffective, leading to similar deactivation in CO production Faradaic efficiency from ~40% to ~16% (Figure S4).

Seeking an alternative to preelectrolysis methods, we envisioned that introducing EDTA to C_i electrolytes would prevent metal deposition, thereby, enhancing long-term catalysis. CV scans of a Au electrode recorded immediately following 45 minutes of CDR catalysis in C_i electrolyte containing 3.4 μM EDTA (Figure 1F, red) do not exhibit the Zn and Cu stripping features observed for the same experiment conducting in the absence of EDTA (Figure 1F, green). We also do not observe Zn and Cu features by XPS after 45 min of CDR catalysis in EDTA-containing electrolyte (Figure 1C, red), indicating an impurity free surface. A broad oxidative feature is observed beginning at 0.60 V (Figure 1F, red), which we attribute to the oxidation of surface adsorbed CO formed during electrolysis.[58] We speculate that in untreated electrolytes, this weak feature is masked by the copper stripping wave.

In line with the absence of metal fouling observed by CV, we find that *ex situ* and *in situ* metal ion chelation significantly attenuates catalyst deactivation. Au electrodes display sustained CDR activity when operated in C_i electrolyte containing 3.4 μM EDTA (Figure 2A, red circles). The concentration of EDTA was chosen based on the M^{2+} impurity concentration measured by ICP-MS of native C_i electrolyte. The initial Faradaic efficiency for CO production is ~80% with only a slight decay to ~70% after two hours of steady state electrolysis. Further enhancement in catalytic activity is afforded by purification of C_i electrolyte with solid-supported iminodiacetate resin (Chelex) prior to electrolysis; CO production on Au is sustained at ~80% over two hours (Figure 2A, blue triangles). In addition, the use of EDTA-containing or Chelex-treated C_i electrolyte enables greater reproducibility in product selectivity and catalyst activity, as evidenced by tighter errors bars

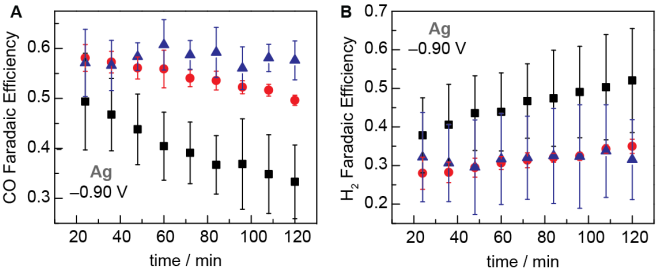

Figure 3: Faradaic efficiencies for CDR and HER product formation on silver foil in electrolytes of varying purity. Activity of Ag for CO (**A**) and H2 (**B**) formation at −0.90 V in native Ci electrolyte (**black squares**), C_i electrolyte containing 3.4 μM EDTA (**red circles**), and Chelex-treated C_i electrolyte (**blue triangles**).

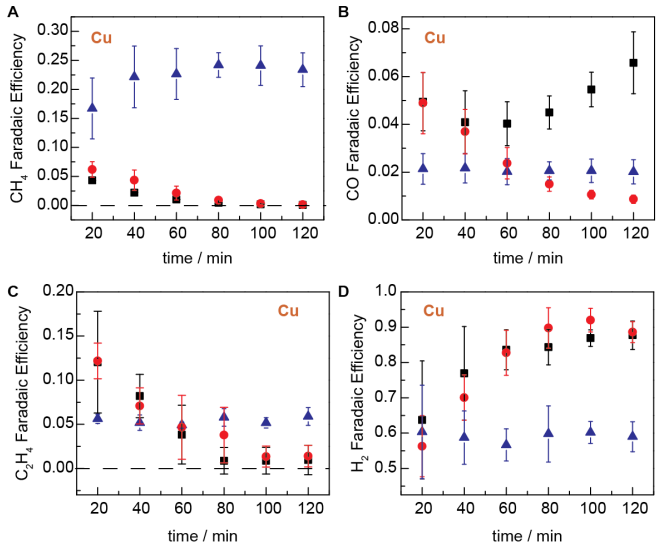

Figure 4: Faradaic efficiencies for CDR and HER product formation on copper foil in electrolytes of varying purity. Activity of Cu for CH4 (**A**), CO (**B**), C2H4 (**C**) and H2 (**D**) formation at −1.00 V in native Ci electrolyte (**black squares**), C_i electrolyte containing 3.4μM EDTA (**red circles**), and Chelex-treated C_i electrolyte (**blue triangles**).

compared to the data obtained from native C_i electrolyte. Furthermore, the sustained CDR selectivities for Au are reflected in sustained partial current densities for CO (Figures S5A) and H_2 production (Figure S5B), indicating that impurity chelation provides for sustained intrinsic rates of product formation. Upon treatment of the electrolyte with either EDTA or Chelex, the current densities for CO production remains high (1.2 $mAcm^{-2}$) relative to HER (0.1 $mAcm^{-2}$). Taken together with the CV and XPS data highlighted above, these results suggest that impurity metal deposition over the course of CDR catalysis is the principal source of electrode deactivation on Au.

Silver electrodes display similar deactivation profiles when operated in native C_i electrolyte. At −0.90 V, CO production on Ag in native C_i electrolyte commences with ~50% Faradaic efficiency but declines over the course of two hours to ~33% (Figure 3A, black squares). This deactivation is accompanied by a corresponding rise from ~38 to ~52% in current going to the HER over the same period. Similar to the results observed on Au, following 45 minutes of CDR catalysis in C_i electrolyte containing 3.4 μM EDTA, no stripping waves are observed by CV (Figure 1E, red) and XPS spectra show no Zn or Cu peaks (Figure 1B, red), indicating a metal impurity free surface. The trailing cathodic feature ending at −0.15 V is attributed to residual catalytic current, and is not observed in subsequent scans.

Consistent with the CV data, EDTA enables sustained and improved CO production, commencing at ~58% and declining only slightly to 52% after two hours of electrolysis (Figure 3B, red circles). As for Au, further enhancements in long-term catalytic activity are observed for C_i electrolytes purified by treatment with Chelex prior to electrolysis: CO production on Ag is sustained at ~60% over the entire two-hour period (Figure 3A, blue triangles). Consistent with the retention in FE, the total currents for product formation are preserved at 0.65 mA cm^{-2} for CO (Figure S6A) and at 0.4 mA cm^{-2} for H_2 formation (Figure S6B). The error bars for the Ag data are large possibly due to variance in the sulfuric acid etching treatment prior to each run. As for Au electrodes, these results suggest that impurity metal deposition during CDR catalysts is the principal source of deactivation of Ag electrodes.

Copper electrodes display complex deactivation profiles when operated at −1.00 V in native C_i electrolyte. At early times, the principal gas phase CDR product is C_2H_4 with ~12% Faradaic efficiency, Figure 4C. However, after two hours of electrolysis this C_2 product is not observed at all. Similarly, CH_4 production commences at ~7% Faradaic efficiency, but is not observed after two hours of electrolysis, Figure 4A. The decline in selectivity for higher order CDR products is accompanied by a rise in H_2 production yield from ~65% to ~85%, Figure 4D. These results are consistent with previous reports of Cu at similar potentials.[35] Over the same time period, the minority production of CO, ~5%, remains constant within error over the two hour electrolysis period, Figure 4B. We only examine gas phase products in this study, and note that copper also mediates the production of liquid products including ethanol, propanol and formate,[23] under these conditions.

The data obtained in the case of Cu differ from those collected when using Ag and Au; we do not observe enhanced long-term CDR activity on Cu electrodes operated in EDTA containing C_i electrolyte. The deactivation profiles for C_2H_4 and CH_4 production as well as the rise in H_2 production are similar to that observed for native C_i electrolyte (Figures 4A, 4C, 4D, red circles). Surprisingly, the introduction of EDTA to the electrolyte promotes a decline in CO production Faradaic efficiency from ~5% to ~0% over the course of two hours, Figure 4B. While these observations seem to imply that EDTA is ineffective at preventing metal deposition on Cu electrode surfaces, voltammetry scans recorded immediately following 2 hours of electrolysis in the presence of EDTA do not display any stripping waves (Figure 1D, red), and XPS spectra recorded following electrolysis show no Zn or Pb peaks (Figure 1A, red), suggesting a metal impurity free surface. The trailing cathodic feature ending at 0.00 V is attributed to residual catalytic current, and is not observed in subsequent scans. Based on these results, we propose that the observed inefficacy of EDTA in preventing CDR deactivation on Cu may result from direct interaction of the chelator with the surface and/or chelator-induced surface restructuring. Interestingly, the rise in CO production observed for Cu operated in native C_i electrolyte, which is not seen in EDTA-containing C_i electrolyte, suggests that Pb or Zn metal deposition, observed by XPS (Figure 1A) and CV (Figure 1D), may promote release of CO intermediates from Cu surfaces.

The observed deactivation of Cu electrodes can, however, be eliminated by pre-treatment of C_i electrolyte with Chelex. The principal CDR product is CH_4 with ~20% Faradaic efficiency sustained over two hours (Figure 4A, blue triangles). Similarly, C_2H_4 and CO production is sustained at ~5% (Figure 4C, blue triangles) and ~2% (Figure 4B, blue triangles), respectively, over the same time period. It appears that removal of metal ion impurities from the electrolyte alters product selectivity even at early reaction times, as shown by the substantial enhancement in methane yield and corresponding decrease in C_2H_4 Faradaic efficiency.

Importantly, the sustained CDR selectivities described above for Cu are reflected in sustained partial current densities for CO_2 reduction products, including CH_4 (Figure S7A), CO

(Figure S7B), C_2H_4 (Figure S7C), and H_2 (Figure S7D). These results indicate that impurity chelation provides for sustained intrinsic rates of CDR product formation. Thus, the methods described here may prove particularly valuable for detailed studies of CDR that require temporal fidelity of the catalyst surface.

3. CONCLUSIONS

In summary, we have shown that the commonly observed activity loss of group 11 catalyst for CDR arises principally from impurity metal deposition. Additionally, we have shown that impurity metal deposition can be reduced or eliminated by chelation with EDTA or electrolyte purification via treatment with a solid-supported metal chelating resin. The results highlight the extremely high sensitivity of CDR to metal ion impurities and the value of post-electrolysis CVs in diagnosing impurity-assisted fouling. The simple approach described here establishes an accessible general protocol for evaluating CO_2 reduction and other fuel forming electrocatalysts under conditions that preserve the fidelity of the native surface.

ASSOCIATED CONTENT

Supporting Information.
Full experimental details, survey XPS spectra, stripping voltammetry experiments in the presence of various M^+ salts, and intrinsic rates of CO_2 reduction product formation in electrolytes of different purities. This material is available free of charge via the Internet at http://pubs.acs.org.

AUTHOR INFORMATION

Corresponding Author

*yogi@mit.edu

ACKNOWLEDGMENT

The authors gratefully acknowledge Melissa Zastrow for assistance with purification protocols. This research was supported by the Aramco Services Company through an MIT Energy Initiative Grant, the Air Force Office of Scientific Research under award FA9550-15-1-0135, and by the MIT Department of Chemistry through junior faculty funds for Y.S. A.W. is supported by a predoctoral fellowship from the National Science Foundation. This work made use of the MRSEC Shared Experimental Facilities at MIT, which is supported in part by the NSF under award DMR-0819762.

REFERENCES

(1) Twigg, M. V.; Spencer, M. S. *Top. Catal.* **2003**, *22*, 191–203.

(2) Besson, M.; Gallezot, P. *Catal. Today* **2003**, *81*, 547–559.

(3) Koel, B. E.; Kim, J. In *Handbook of Heterogeneous Catalysis*; G. Ertl, H. Knözinger, F. Schüth, J. W., Ed.; Wiley-VCH: Weinheim, 2008; Vol. 5, pp 1593–1624.

(4) Butt, J.; Peterson, E. E. *Activation, Deactivation, and Poisoning of Catalysts*; Academic Press: San Diego, 1988.

(5) Buchwald, S. L.; Bolm, C. *Angew. Chem. Int. Ed. Engl.* **2009**, *48*, 5586–5587.

(6) Crabtree, R. H. *Chem. Rev.* **2012**, *112*, 1536–1554.

(7) Klug, D.; Rabani, J.; Fridovich, I. *J. Biol. Chem.* **1972**, *247*, 4839–4842.

(8) Peracchi, A. *Trends Biochem. Sci.* **2001**, *26*, 497–503.

(9) Lee, S. H.; Ha, S. H.; Lee, S. B.; Koo, Y.-M. *Biotechnol. Lett.* **2006**, *28*, 1335–1339.

(10) Ullman, A. M.; Liu, Y.; Huynh, M.; Bediako, D. K.; Wang, H.; Anderson, B. L.; Powers, D. C.; Breen, J. J.; Abruña, H. D.; Nocera, D. G. *J. Am. Chem. Soc.* **2014**, *136*, 17681–17688.

(11) Corrigan, D. A. *J. Electrochem. Soc.* **1987**, *134*, 377–384.

(12) Trotochaud, L.; Young, S. L.; Ranney, J. K.; Boettcher, S. W. *J. Am. Chem. Soc.* **2014**, *136*, 6744–6753.

(13) Bockris, J. O.; McHardy, J. *J. Electrochem. Soc.* **1973**, *120*, 61–66.

(14) Paulus, U. A.; Schmidt, T. J.; Gasteiger, H. A. In *Handbook of Fuel Cells*; John Wiley & Sons, Ltd: Chichester, 2010.

(15) Wang, L.; Ambrosi, A.; Pumera, M. *Angew. Chem. Int. Ed. Engl.* **2013**, *52*, 13818–13821.

(16) Perez, J.; Gonzalez, E. R.; Villullas, H. M. *J. Phys. Chem. B* **1998**, *102*, 10931–10935.

(17) Kondratenko, E. V.; Mul, G.; Baltrusaitis, J.; Larrazábal, G. O.; Pérez-Ramírez, J. *Energy Environ. Sci.* **2013**, *6*, 3112–3135.

(18) Olah, G. A.; Prakash, G. K. S.; Goeppert, A. *J. Am. Chem. Soc.* **2011**, *133*, 12881–12898.

(19) Whipple, D. T.; Kenis, P. J. A. *J. Phys. Chem. Lett.* **2010**, *1*, 3451–3458.

(20) Rosenthal, J. In *Progress in Inorganic Chemistry*; Karlin, K. D., Ed.; Progress in Inorganic Chemistry; John Wiley & Sons: Hoboken, New Jersey, 2014; pp 299–338.

(21) Benson, E. E.; Kubiak, C. P.; Sathrum, A. J.; Smieja, J. M. *Chem. Soc. Rev.* **2009**, *38*, 89–99.

(22) Hori, Y. In *Modern Aspects of Electrochemistry*; Vayenas, C., White, R., Gamboa-Aldeco, M., Eds.; Modern Aspects of Electrochemistry; Springer, New York, 2008; Vol. 42, pp 89–189.

(23) Hori, Y.; Wakebe, H.; Tsukamoto, T.; Koga, O. *Electrochim. Acta* **1994**, *39*, 1833–1839.

(24) Kuhl, K. P.; Cave, E. R.; Abram, D. N.; Jaramillo, T. F. *Energy Environ. Sci.* **2012**, *5*, 7050–7059.

(25) Hatsukade, T.; Kuhl, K. P.; Cave, E. R.; Abram, D. N.; Jaramillo, T. F. *Phys. Chem. Chem. Phys.* **2014**, *16*, 13814–13819.

(26) Sreekanth, N.; Phani, K. L. *Chem. Commun.* **2014**, *50*, 11143–11146.

(27) Peterson, A. A.; Nørskov, J. K. *J. Phys. Chem. Lett.* **2012**, *3*, 251–258.

(28) Calle-Vallejo, F.; Koper, M. T. M. *Angew. Chem. Int. Ed. Engl.* **2013**, *52*, 7282–7285.

(29) Montoya, J. H.; Peterson, A. A.; Nørskov, J. K. *ChemCatChem* **2013**, *5*, 737–742.

(30) Nie, X.; Esopi, M. R.; Janik, M. J.; Asthagiri, A. *Angew. Chem. Int. Ed. Engl.* **2013**, *52*, 2459–2462.

(31) Peterson, A. A.; Abild-Pedersen, F.; Studt, F.; Rossmeisl, J.; Norskov, J. K. *Energy Environ. Sci.* **2010**, *3*, 1311–1315.

(32) Kedzierzawski, P.; Augustynski, J. *J. Electrochem. Soc.* **1994**, *141*, L58–L60.

(33) Jermann, B.; Augustynski, J. *Electrochim. Acta* **1994**, *39*, 1891–1896.

(34) Kostecki, R.; Augustynski, J. *Berichte der Bunsengesellschaft für Phys. Chemie* **1994**, *98*, 1510–1515.

(35) Hori, Y.; Konishi, H.; Futamura, T.; Murata, A.; Koga, O.; Sakurai, H.; Oguma, K. *Electrochim. Acta* **2005**, *50*, 5354–5369.

(36) Yano, H.; Shirai, F.; Nakayama, M.; Ogura, K. *J. Electroanal. Chem.* **2002**, *533*, 113–118.

(37) Chen, Y.; Li, C. W.; Kanan, M. W. *J. Am. Chem. Soc.* **2012**, *134*, 19969–19972.

(38) Kas, R.; Kortlever, R.; Yılmaz, H.; Koper, M. T. M.; Mul, G. *ChemElectroChem* **2015**, *2*, 354–358.

(39) DeWulf, D. W.; Jin, T.; Bard, A. J. *J. Electrochem. Soc.* **1989**, *136* , 1686–1691.

(40) Wasmus, S.; Cattaneo, E.; Vielstich, W. *Electrochim. Acta* **1990**, *35*, 771–775.

(41) Kyriacou, G.; Anagnostopoulos, A. *J. Electroanal. Chem.* **1992**, *322*, 233–246.

(42) Hoogvliet, J. C.; Dijksma, M.; Kamp, B.; van Bennekom, W. P. *Anal. Chem.* **2000**, *72*, 2016–2021.

(43) Batista, E. A.; Temperini, M. L. A. *J. Electroanal. Chem.* **2009**, *629*, 158–163.

(44) Lu, Q.; Rosen, J.; Zhou, Y.; Hutchings, G. S.; Kimmel, Y. C.; Chen, J. G.; Jiao, F. *Nat. Commun.* **2014**, *5*, 3242.

(45) Li, C. W.; Kanan, M. W. *J. Am. Chem. Soc.* **2012**, *134*, 7231–7234.

(46) Furia, T. E. In *CRC Handbook of Food Additives*; Furia, T. E., Ed.; CRC Press: Boca Raton, 1972; pp 271–294.

(47) Eigen, M.; Wilkins, R. G. *Mechanisms of Inorganic Reactions*; Kleinberg, J., Murmann, R. K., Fraser, R. T. M., Bauman, J., Eds.; Advances in Chemistry; American Chemical Society: Washington, D.C., 1965; Vol. 49, pp 55–80.

(48) Bril, K.; Bril, S.; Krunhotz, P. *J. Phys. Chem.* **1956**, *60*, 251–252.

(49) Bril, K.; Bril, S.; Krumholz, P. *J. Phys. Chem.* **1955**, *59*, 596–600.

(50) Tanaka, N.; Osawa, H.; Kamada, M. *Bull. Chem. Soc. Jpn.* **1963**, *36*, 530–534.

(51) Vanýsek, P. *CRC Handbook of Chemistry and Physics*, 95th ed.; Haynes, W. M., Ed.; CRC Press: Boca Raton, 2014.

(52) Brisard, G. M.; Zenati, E.; Gasteiger, H. A.; Marković, N. M.; Ross, P. N. In *Solid-Liquid Electrochemical Interfaces*; Jerkiewicz, G., Soriaga, M. P., Uosaki, K., Wieckowski, A., Eds.; ACS Symposium Series; American Chemical Society: Washington, D.C., 1997; Vol. 656, pp 142–155.

(53) Takahashi, S.; Hasebe, K.; Aramata, A. *Electrochem. Commun.* **1999**, *1*, 301–304.

(54) Adzic, G. *J. Electrochem. Soc.* **1981**, *128*, 1691–1697.

(55) Chu, M. G. *J. Electrochem. Soc.* **1981**, *128*, 2281–2286.

(56) Fonticelli, M. H.; Posadas, D.; Tucceri, R. I. *J. Electroanal. Chem.* **2004**, *565*, 359–366.

(57) Gerischer, H.; Kolb, D. M.; Przasnyski, M. *Surf. Sci.* **1974**, *43*, 662–666.

(58) Kita, H.; Nakajima, H.; Hayashi, K. *J. Electroanal. Chem. Interfacial Electrochem.* **1985**, *190*, 141–156.

SYNOPSIS TOC